Development of Lightweight X-Ray Mirrors for the Constellation-X Mission

William W. Zhang, Kai-Wing Chan*, David A. Content,
John P. Lehan*, Robert Petre, and Timo T. Saha
NASA's Goddard Space Flight Center, Greenbelt, MD 20771 USA
Mikhail Gubarev*, William D. Jones, and Stephen L. O'Dell
NASA's Marshall Space Flight Center, Huntsville, AL 35812 USA
* *Also* Universities Space Research Association

ABSTRACT

Constellation-X is NASA's next major X-ray observatory. It requires X-ray mirrors with high throughput (3 m^2 effective area at 1 keV), moderate angular resolution (15″ half power diameter), and light weight (about an order of magnitude lighter than XMM/Newton's). Over the past few years we have been developing a glass forming technology for making mirrors. This technology by construction meets from the outset two (throughput and weight) of the three requirements. Our development effort has been concentrated on improving the angular resolution. Our progress so far has shown that this technology not only can meet the angular resolution requirement of 15″ HPD, but also has the potential to reach Constellation-X's goal of 5″ HPD. This paper is a snapshot of our X-ray mirror development effort as of May 2006. It briefly describes the mirror fabrication process, results achieved, and important issues that are being worked on.

Keywords: X-ray optics, lightweight optics, Constellation-X, space optics

1. INTRODUCTION

Constellation-X is NASA's next major X-ray observatory (White et al. 2006). It is designed to have two sets of X-ray telescopes: the spectroscopic X-ray telescopes (SXT) (Petre et al. 2006) and the hard X-ray telescopes (HXT). The SXT includes four identical mirror assemblies, each of which is 1.6m in diameter and has a 10m focal length, and has its own micro-calorimeter array (Kelley et al. 2006) and grating array (Cottam 2006). This paper reports on the development of X-ray mirror segments that can be used for both SXT and HXT. Their alignment and integration into full mirror assemblies are reported elsewhere (Owens et al. 2006 and Zhang et al. 2006).

The challenge of making SXT mirrors can be appreciated by comparing them with those of other missions in terms of four parameters: angular resolution, effective area, mirror areal density, and production cost. Table 1 presents a comparison of the SXT requirements with those of the three currently operating missions, which represent the state of the art of X-ray optics manufacturing. Compared to XMM/Newton, Con-X mirrors need to 8 times lighter while maintaining the same angular resolution. Compared to Chandra, they have a 30 times lower angular resolution, but have to be more than 150 times lighter. Compared to Suzaku, they are 2 times heavier, but have to be 8 times better in angular resolution. Given their unprecedented amount of physical area, the Con-X mirrors have to be manufactured at a much lower cost per unit area to make the mission financially feasible in a budget-constrained environment.

Space Telescopes and Instrumentation II: Ultraviolet to Gamma Ray, edited by
Martin J. L. Turner, Günther Hasinger, Proc. of SPIE Vol. 6266, 62661V, (2006)
0277-786X/06/$15 · doi: 10.1117/12.672138

In the past several years we have been developing a thermal glass forming technique. The thrust of our development program has been to improve the precision of the forming process to meet the angular resolution requirement.

The mirror fabrication process starts with a thin (0.4mm) flat glass sheet. It is placed atop a convex mandrel as shown in Figure 1. It is then heated in an oven to a high temperature so that it slumps under its own weight and conforms to the figure of the mandrel. The forming process has been described in previous publications (Zhang et al. 2003, 2004a, 2004b, and 2005).

Table 1. Comparison of the Con-X SXT with the mirrors of three operating missions, representing the state of the art of X-ray optics fabrication and integration.

	Con-X/SXT	**Chandra**	**XMM/Newton**	**Suzaku**
No. of mirror assemblies	4	1	3	5
No. of shells per assembly	216	4	58	168
Total mirror physical area (m^2)	890	19	158	125
Angular resolution at 1 keV (″ HPD)	15	0.5	15	120
Mirror Technology	Thermally formed float glass segments	Ground and polished Zerodur shells	Electroformed nickel shells	Epoxy replicated aluminum segments
Typical mirror areal density (g/m^2)	1	~150	8	0.5
Mirror manufacturing Cost per unit area	Low	Extremely expensive	Moderate	Moderate to Low
Year of Launch	2018 (?)	1999	1999	2005

This approach is a replication process. As such it does not depend on precision metrology, which is both time-consuming and expensive. In particular, we have found that the slumping process preserves the excellent microroughness of the float glass sheets.

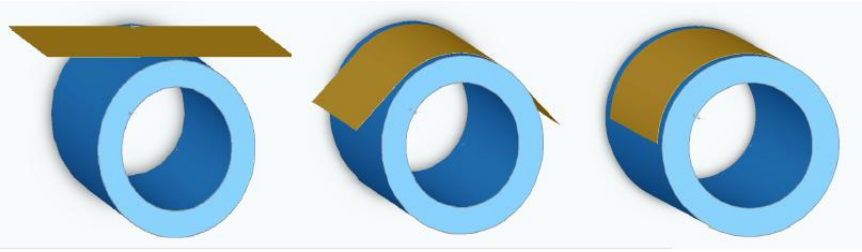

Figure 1. An illustration of the mirror forming process. Time and temperature progress from left to right. The whole process takes place inside an electric oven meeting stringent temperature uniformity requirements.

2. STATUS OF MIRROR SEGMENT FABRICATION

Like other replication process, the glass forming process is susceptible to both random and systematic errors. Random error, by definition, is not repeatable from one mirror to the next. Systematic error represents repeatable deviation of the mirror from the mandrel. It is introduced in the forming process or the metrology process in deterministic ways. In this section we present results to show that our glass forming process is a highly reproducible process with very little random error. We also show that we have identified systematic errors contributed by both the forming process and the metrology process. Now first we set up a coordinate system and outline the parameters we need to measure to completely characterize a mirror segment.

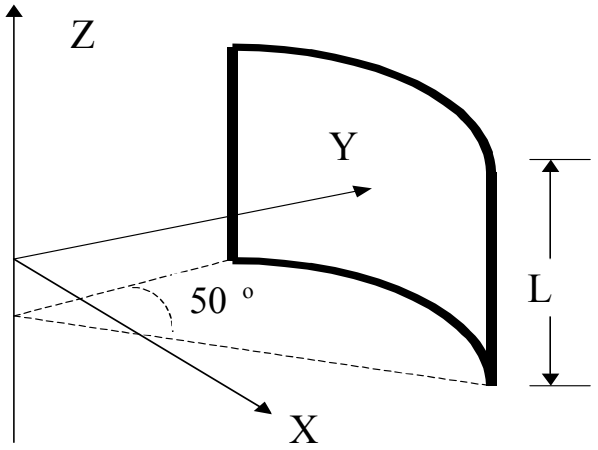

Figure 2. Coordinate system used for defining the mirror segment.

For convenience and ease of visualization, the standard Wolter-I prescription of a mirror, either parabolic or hyperbolic, can be generalized and written as

$$\rho(z,\phi) = \rho_0(\phi) + z \cdot \tan\theta(\phi) - \left(\frac{2z}{L}\right)^2 \cdot s(\phi) + R(z,\phi), \qquad (1)$$

where $\rho^2 = \sqrt{x^2 + y^2}$, in the coordinate system as defined in Figure 2. The segment mirror in the present context is defined in the region

$$-\frac{L}{2} \le z \le \frac{L}{2}, \quad L = 200 \text{ mm; and } \; 0^o \le \phi \le 50^o.$$

For a practically perfect Wolter-I mirror, of course, all the dependence on azimuthal angle and the fourth term vanish. Eq. (1) describes a real-world mirror whose various errors can be defined and measured as follows.

AVERAGE RADIUS AND ROUNDNESS ERROR The first term in Eq (1) can be further rewritten as $\rho_0(\phi) = \rho_0 + \Delta\rho_0 + \Delta\rho(\phi)$, (2)

where ρ_o is azimuth-independent and represents the design radius; $\Delta\rho_o$, also azimuth-independent, represents the deviation from the design value; and $\Delta\rho(\phi)$, by definition, having a zero mean, represents the in-phase out-of-roundness.

AVERAGE CONE ANGLE ERROR AND CONE ANGLE VARIATION Similarly the cone angle in the second term in Eq. (1) can be rewritten as

$$\theta(\phi) = \theta_0 + \Delta\theta_0 + \Delta\theta(\phi), \qquad (3)$$

where θ_o is azimuth-independent and the design cone angle; $\Delta\theta_o$, also azimuth-independent, represents the deviation from the design value; and $\Delta\theta(\phi)$, by definition, having a zero mean, represents any cone angle variation as a function of azimuth.

AVERAGE SAG ERROR AND SAG VARIATION Similarly the sag term in Eq. (1) can also be rewritten as

$$s(\phi) = s_0 + \Delta s_0 + \Delta s(\phi), \qquad (4)$$

where s_o is azimuth-independent and the design sag; Δs_o, also azimuth-independent, represents the deviation from the design sag; and $\Delta s(\phi)$, by definition, having a zero mean, represents any sag variation as a function of azimuth.

AXIAL FIGURE ERROR The last term in Eq. (1), $R(z,\phi)$, represents the rest of the deviation of the real-world mirror from that of a mathematically perfect mirror. Again by definition, this term has a zero mean. It is important to note that the grazing incidence nature of the X-ray optics determines that the variation of $R(z,\phi)$ with z is much more important than its variation with azimuth angle ϕ. In other words, we can tolerate a much higher slope error in the azimuth direction than in the z direction. This difference in tolerance can be expressed as

$$\frac{\partial R(z,\phi)}{\partial z} \sim \frac{\alpha}{\rho_o} \cdot \frac{\partial R(z,\phi)}{\partial \phi}, \qquad (5)$$

where α is the grazing angle. Given the fact that in our mirror fabrication process the two independent directions are treated the same, we expect that the variations in the two directions are similar, if not identical. As such we only need to be concerned with the variation in z. Once the requirement on variation in the z direction is met, the variation in the azimuth direction is automatically also met.

Therefore it is only necessary to measure the $R(z,\phi)$ as a function of z at several or many different azimuths, in other words, many axial figure measurements. This is why this term is dubbed the axial figure error, even though it is dependent upon azimuth also.

Although it is not part of the mirror fabrication process, as is the case with the traditional grinding and polishing process, metrology is essential to developing and perfecting the thermal forming process. Quantitative comparison between the parameters and figure of the forming mandrel and those of the formed mirror segment is indispensable. While the metrology of the forming mandrel is relatively straightforward and has been done in the past, the metrology of the formed mirror segment, because of its extraordinary aspect ratio (200mm length/width by 0.4mm thickness) is severely hampered by two additional factors: figure distortion caused by gravity and by any mounting structure. Table 2 presents an overview of the various parameters and the metrology equipment being used to measure them. In particular, the "Challenge" and "Status" columns show the difficulties and results we have obtained so far.

RANDOM ERROR (OR REPRODUCIBILITY OF THE FORMING PROCESS) Figure 4 shows a comparison of two consecutively formed mirror segments. The black and blue curves represent axial scans of the two mirror segments measured of the same meridians. It is clear that they track each other very well. The difference between the two sets of curves is about 30nm RMS, amounting to a nominal forming random error of $30/\sqrt{2} = 21$ nm. It is worth noting that this number should be considered an upper limit for two reasons. First, the cross registration between the two mirror segments is far from being perfect. Any registration error tends to show up as non-repeatability. Second, this number contains metrology "noise" in the sense that consecutive measurements of the same mirror segment at the "same" spot give a comparable difference RMS.

SYSTEMATIC ERROR At present we use an operational or somewhat ad hoc definition of systematic error. It is the difference in figure between the forming mandrel and the formed mirror segment that cannot be accounted for by the random error defined above. As such, the systematic error includes both error associated with the fabrication process and error associated with the metrology process. This is necessary for the simple reason that it is not always easy, if possible, to separate the two errors.

The left panels of Figures 5 and 6 show comparisons of two mirror segments and their corresponding forming mandrels. A couple of precautions are in order. First, since the cross registration between the mirror segment and the forming mandrel has been done with an accuracy of about 1 mm, some mismatch of fine features is expected even if the mirror segment is perfectly formed. Second, the grass-like ripples of the mandrel curves are due to metrology noise and should be excluded from consideration. With these precautions in mind, we see that the mirror segments match the mandrels very well in the low spatial frequency regime. We can also see clearly that the mirror segments tend to have more mid-frequency ripples than the mandrels. We can also see these features on the right panels of Figure 5 and 6, which show the corresponding power spectral densities. Quantitative comparisons can be made in the following three spatial frequency bands:

1. **$0.005\ \text{mm}^{-1} < f < 0.05\ \text{mm}^{-1}$ (or spatial periods from 200 mm to 20 mm):** As Figures 5 and 6 show, the mirror segment and its corresponding mandrel have essentially the same figure, evidencing the fidelity of the thermal forming process. This is typically the case, but not always the case. It is highly likely that any apparent difference between the two figures in this frequency band us caused by gravity and metrology mount distortion. The final resolution awaits further investigation.

2. **$0.05\ \text{mm}^{-1} < f < 0.5\ \text{mm}^{-1}$ (or spatial periods from 20 mm to 2 mm):** In general the mirror segment's apparent figure is substantially worse than that of the mandrel's. There are two reasons for this. The first one is due to a release layer on the mandrel, which probably has degraded the mandrel figure in this band. The second reason is that the off-axis parabola beam expander, as shown in Figure 3, contributes about 30% of the error because of its polishing marks.

3. **$f > 0.5\ \text{mm}^{-1}$ (or spatial periods shorter than 2 mm):** Part of this band has been measured (spatial periods from 1 μm to 300 μm) to have satisfactory microroughness. It shows that the thermal forming process does not degrade the microroughness in this band. The rest of the band, spatial periods from 300 μm to 2 mm has not be been adequately measured because of lack of equipment. We are in the process of procuring a Zygo surface profiler that is capable of covering this band.

Table 2. Mirror parameters and their measurement techniques, challenges associated with their measurement, and the status of our work. This paper focuses on the two rows highlighted in red.

Mirror Parameter		Metrology Equipment	Challenge	Comment	Status
Radius	Average Radius ($\rho_0 + \Delta\rho_0$)	Cylindrical coordinate measuring machine	Gravity distortion Mount distortion	Single number	Work in progress; Current measurements unreliable due to gravity and mount distortion
	Radius Variation ($\Delta\rho(\phi)$)			Having frequency content	
Cone Angle	Average Cone Angle ($\theta_0 + \Delta\theta_0$)			Single number	
	Cone Angle Variation ($\Delta\theta(\phi)$)			Having frequency content	
Axial Figure	Average Sag ($S_0 + \Delta S_0$)	Fizeau phase measuring interferometer, as shown in Figure 3	Gravity distortion Mount distortion	Single number	Current measurements unreliable due to gravity and mount distortion
	Sag Variation ($\Delta S(\phi)$)			Having frequency content	
	Low Frequency Figure (0.005 – 0.05 mm^{-1}) or (200 – 20 mm period)			Having frequency content	**Current measurements probably affected by gravity and mount distortion**
	Middle Frequency Figure (0.05 – 0.5 mm^{-1}) or (20 – 2 mm period)		Reference optics figure error	Having frequency content	**Current measurements slightly affected by mid-frequency errors on reference optics**
	High Frequency Figure (> 0.5 mm^{-1}) or (< 2 mm period)	Interferometric surface profiler	None	Having frequency content	Work in progress

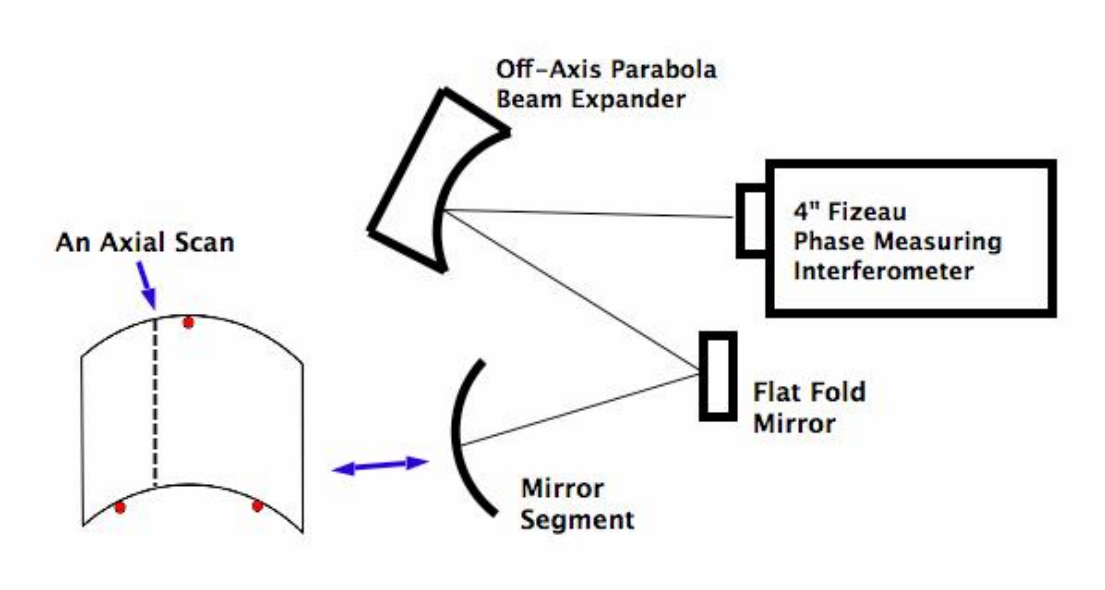

Figure 3. Schematic of the metrology setup to obtain the data reported in this paper. During the measurement, the mirror segment is standing on two points at the bottom and held in balance at a third point at the top.

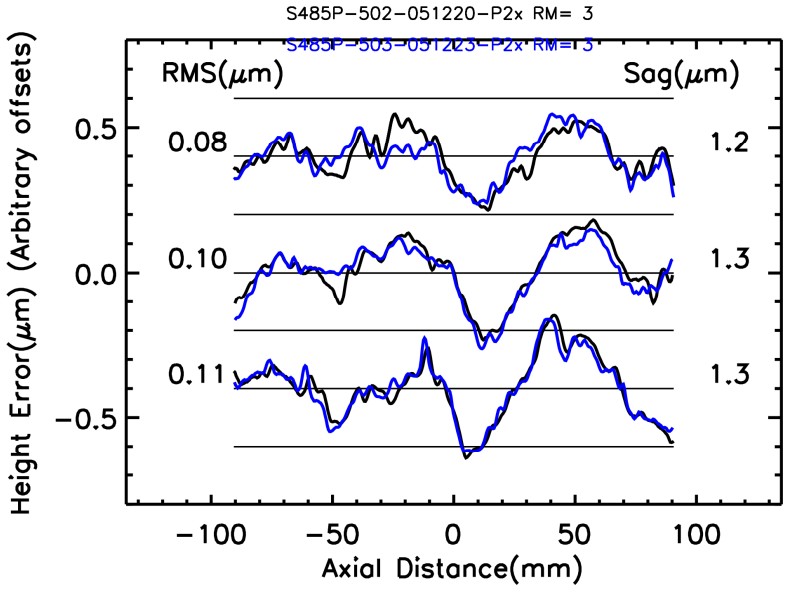

Figure 4. Axial scans of two consecutively formed mirrors, showing the high degree of repeatability of the forming process. A second order polynomial has been removed before plotting. The P-V value of the second order is listed under the Sag column.

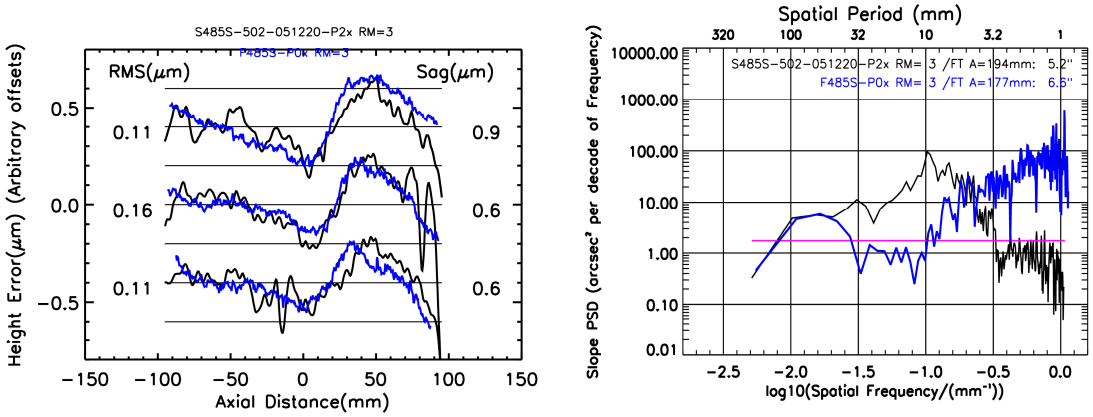

Figure 5. Left Panel: Axial scans of a mirror segment (black) with the same scans of the mandrel's (blue) superposed. A second order polynomial has been removed before plotting. The P-V value of the second order is listed under the Sag column. **Right Panel:** The corresponding power spectral densities. The purple line represents the nominal requirement of the SXT.

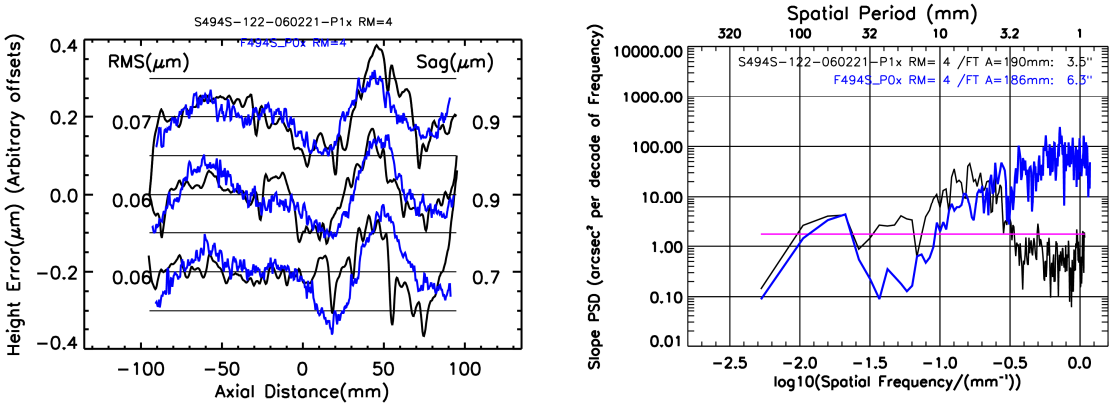

Figure 6. The same as those in Figure 5, except that these are for another mirror segment formed off a different mandrel. Note that the vertical scale of the left panel is a factor of 2 smaller than that of Figure 5.

3. PROBLEMS, SOLUTIONS, AND PROSPECTS

In the last section we used axial figure measurements to illustrate the precision of the glass forming technique. Two conclusions are in order. First, the glass forming technology represents a new optical fabrication technology that is capable of not only meeting SXT requirements, but also, in all likelihood, exceeds them. Second, our knowledge of the process and the formed mirror segments is limited by our ability to measure them. The most important factor is gravity distortion and distortion associated with mounting the mirror for metrology. Here we list the challenges that we must meet in the next year or so to significantly advance this technology.

The first challenge we must meet is to find a way to mount a mirror segment to minimize gravity and friction distortion so that we can measure its true and "free-standing" figure. To this end, we are developing a mirror segment mattress (Zhang et al. 2006) that supports a mirror segment using hundreds very soft springs. We hope that it will enable the measurement of the mirror segment's radius, cone angle, and sag, which we have not been able to do with the three-point mount shown in Figure 3. In particular, we hope that it will allow us to investigate whether gravity and/or mount distortion also contributes significantly to the low frequency figure error.

The second challenge is to reduce or even eliminate the mid-frequency error that currently dominates the mirror performance. We will replace the off-axis parabola beam expander with a new Fizeau interferometer that has a 10 inch beam, thus totally eliminating the wavefront error associated with the measurement optics. We will implement a new mandrel release layer coating technique that is expected to substantially reduce the ripples left on the mandrel surface.

We expect that, once we can adequately measure the mirror substrate and once we substantially reduce the mid-frequency error, we will be able to demonstrate that we can fabricate mirror segments that are as good as our current forming mandrels, which have an angular resolution of approximately 7″ HPD for two reflections, exceeding the Constellation-X SXT requirements. When higher quality forming mandrels become available, we will be able to investigate the possibility of reaching the 5″ HPD goal.

4. ACKNOWLEDGEMENTS

The work reported here results from the hard work of many people at several institutions and companies. While it is not possible to list all their names, we would like to especially acknowledge the contributions of James Mazzarella, Marton Sharpe, David Colella, Melinda Hong, and Theo Hadjimichael. Their dedicated technical support has been indispensable in achieving the results reported here. This work has been financially supported in part by NASA through the Constellation-X Project Office at the Goddard Space Flight Center and through an Astronomy and Physics Research and Analysis (APRA) grant.

REFERENCES

1. Cottam, J., 2006, in these proceedings
2. Kelley, R.L., 2006, in these proceedings
3. Owens, S. et al. 2006, in these proceedings
4. Petre, R. et al., 2006, in these proceedings
5. White, N.E. et al. 2006, in these proceedings
6. Zhang, W.W. et al., 2003, Proceedings of the SPIE, Volume 4851, pp. 503-518 (2003). 4851
7. Zhang, W.W. et al., 2004a, Proceedings of the SPIE, Volume 5488, pp. 820-828 (2004). 5488
8. Zhang, W.W. et al., 2004b, Proceedings of the SPIE, Volume 5168, pp. 168-179 (2004). 5168
9. Zhang, W.W. et al., 2005, Proceedings of the SPIE, Volume 5900, pp. 247-257 (2005). 5900
10. Zhang, W.W., et al., 2006, in these proceedings